Postseismic backslip as a response to a sequential elastic rebound of upper plate and slab in subduction zones

Ehsan Kosari[1,2], Matthias Rosenau[1], Thomas Ziegenhagen[1], and Onno Oncken[1,2]

[1] Helmholtz Centre Potsdam, GFZ German Research Centre for Geosciences, Potsdam, Germany.

[2] Department of Earth Sciences, Freie Universität Berlin, Berlin, Germany.

Contents of this file

Text S1 & S2
Figures S1 to S11

Introduction

This supporting information contains additional text and figures supporting the lines of argumentation in the main manuscript.

Text S1.

Effects of the acceleration on the upper plate fault activity

Besides the consequences on the asperities, the accelerated relocking also affects upper-plate shortening and upper-plate fault activity. The antithetic fault in our experiments switches its kinematic mode and acts as a normal fault coseismically due to its location relative to the megathrust earthquake centroid (e.g., deDontney *et al.*, 2012; Li *et al.*, 2014; Xu *et al.*, 2015). This discontinuity inside the upper plate responds to stress perturbation and stress enhancement. When the MSPs are in opposite modes in the heterogeneous system (loading vs. unloading), they cause compressional (postseismically) and extensional (coseismically and/or early postseismically) stress regimes on the two segments of the antithetic upper plate fault, respectively. The high amount of the early postseismic shortening (postseismic/interseismic=20-25%) may increase the stress level in the upper plate, which is consistent with the reported upper-plate seismicity after megathrust earthquakes (e.g., Asano *et al.*, 2011; Toda, Stein and Lin, 2011; Hoskins *et al.*, 2021).
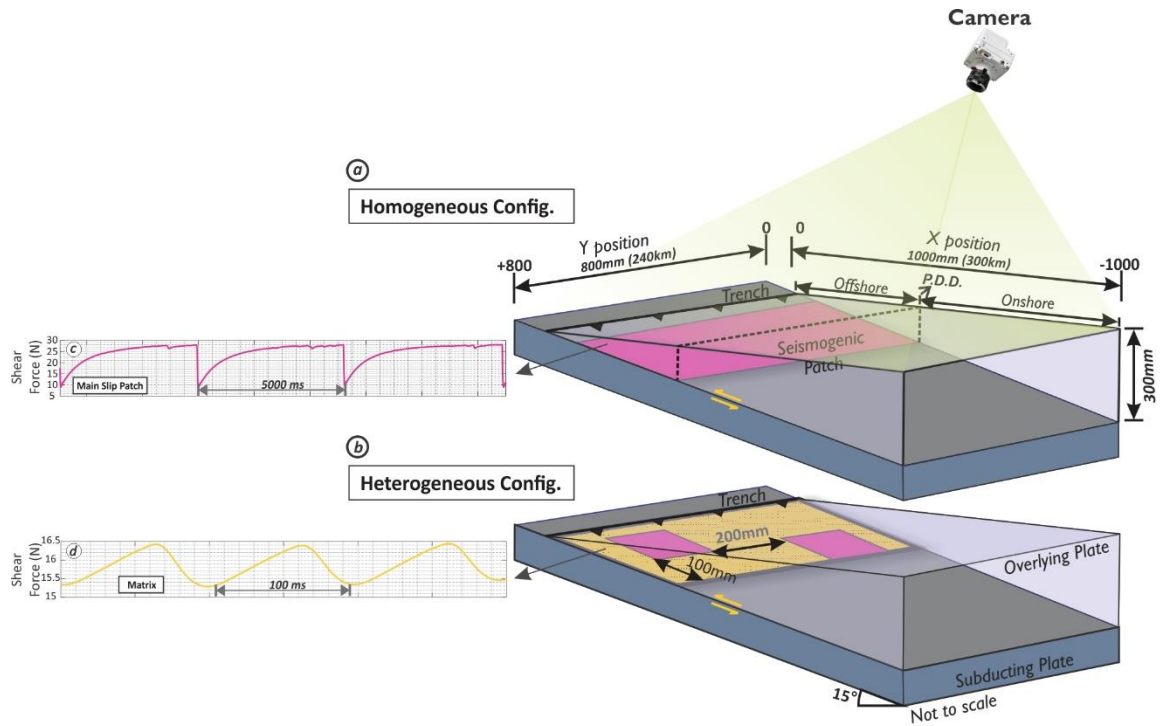
Figure S1. Scheme of the seismotectonic scale model's geometry and configuration; a and b represent homogenous and heterogeneous configurations, respectively. The yellow (matrix) and magenta (main slip patch) rectangles demonstrate the seismogenic patches which generate repeating earthquake and megathrust events, respectively. The magenta (c) and yellow (d) plots (same colors in a and b) demonstrate the behavior of the materials in a ring-shear test under the same normal stress and shear velocity.
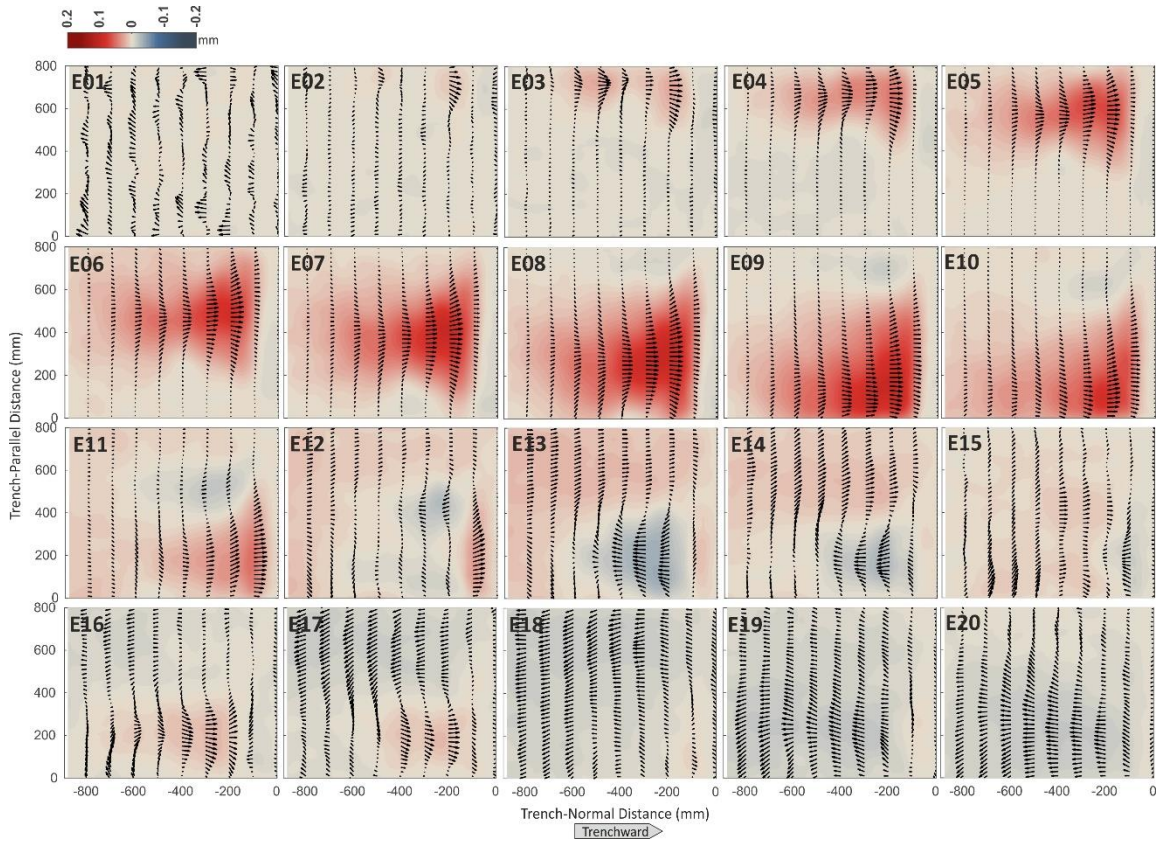
Figure S2. Incremental coseismic and early-postseismic surface displacements of a representative event from the homogenous configuration. The colormap demonstrates the magnitude of the trench-normal displacement. Red and blue color indicate trenchward and rearward ('landward') displacements, respectively.
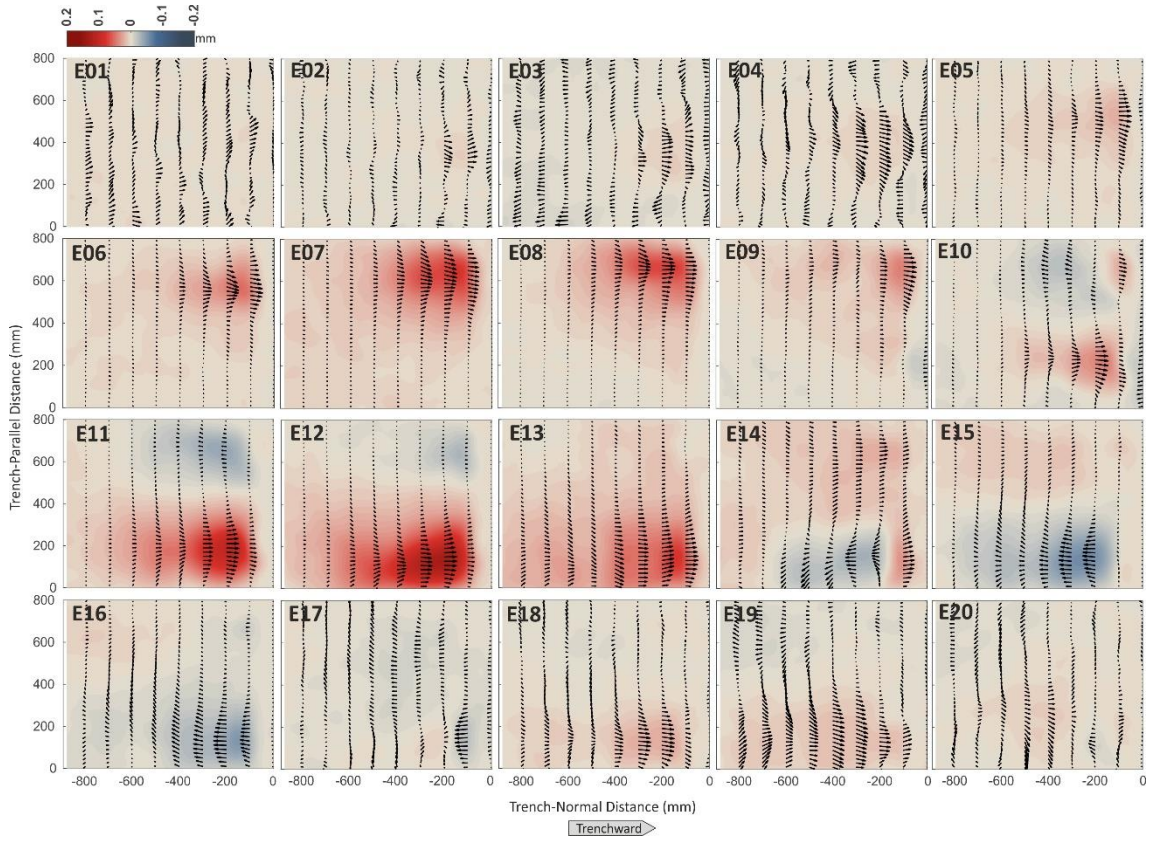
Figure S3. Incremental coseismic and early-postseismic surface displacements of a representative event from the heterogeneous configuration. The colormap demonstrates the magnitude of the trench-normal displacement. Red and blue color indicate trenchward and rearward ('landward') displacements, respectively.
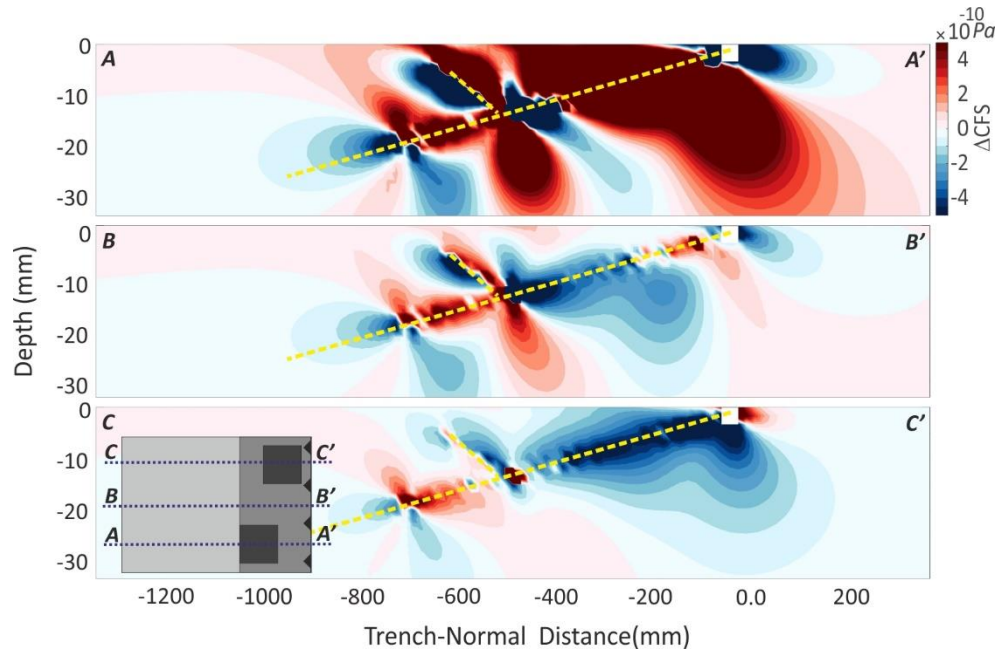
Figure S4. Trench-normal profiles of Coulomb failure stress changes (ΔCFS) on the normal fault receivers derived from the slip model snapshot #12 in the heterogeneous configuration. Inset shows the location of profiles on the model surface.
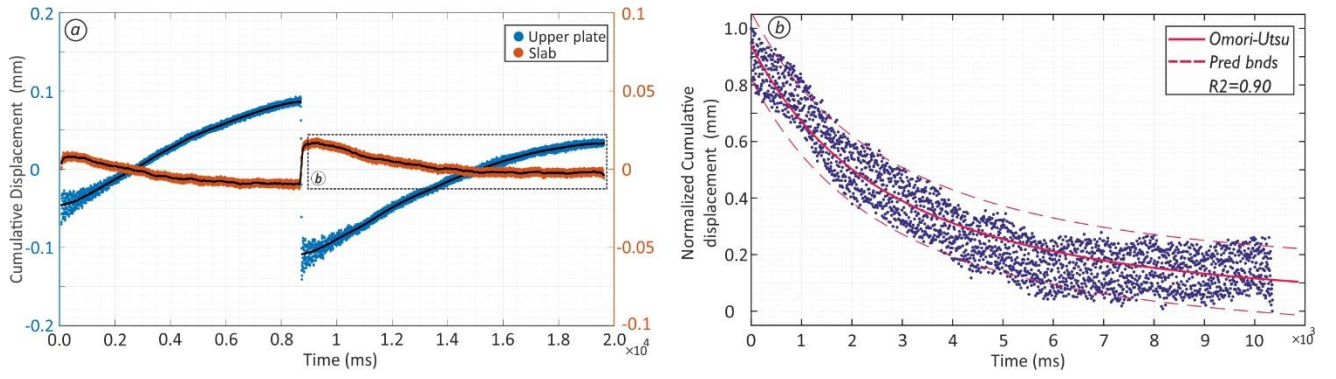
Figure S5. Surface displacement time series of the upper plate and slab in the homogeneous configuration. a) Blue and orange graphs demonstrate the time series of the upper plate and slab, respectively. b) The Omori-Utsu's decay law is fitted to the relaxation section of the slab time-series. The dashed lines indicate the prediction bound of the fit.
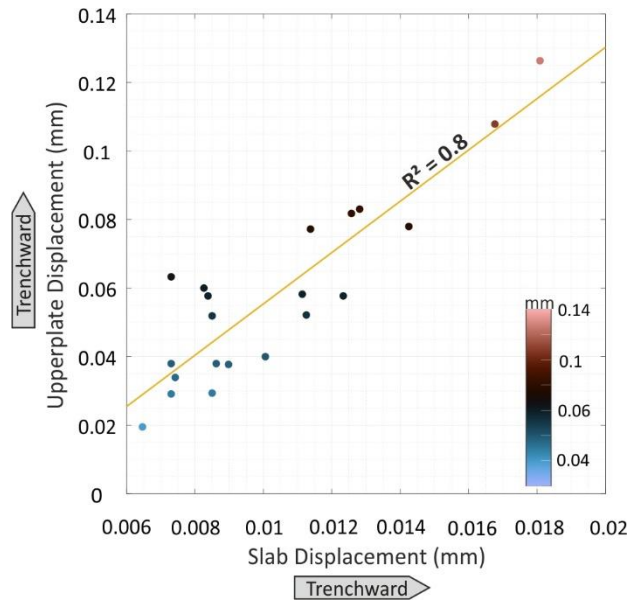
Figure S6. Correlation between the upper plate and slab trenchward (landward) displacements during coseismic and early-postseismic stages.
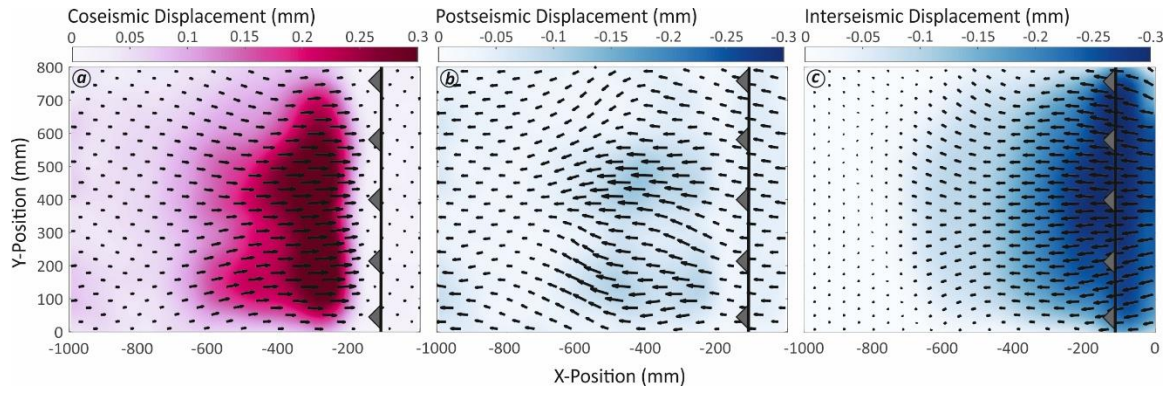
Figure S7. Comparing total trench-normal surface displacement over interseismic (a), coseismic (b), and early-postseismic (c) stages for an event in the homogeneous configuration. The red and blue colormaps represent the magnitude of the trenchwatrd and rearward displacements.
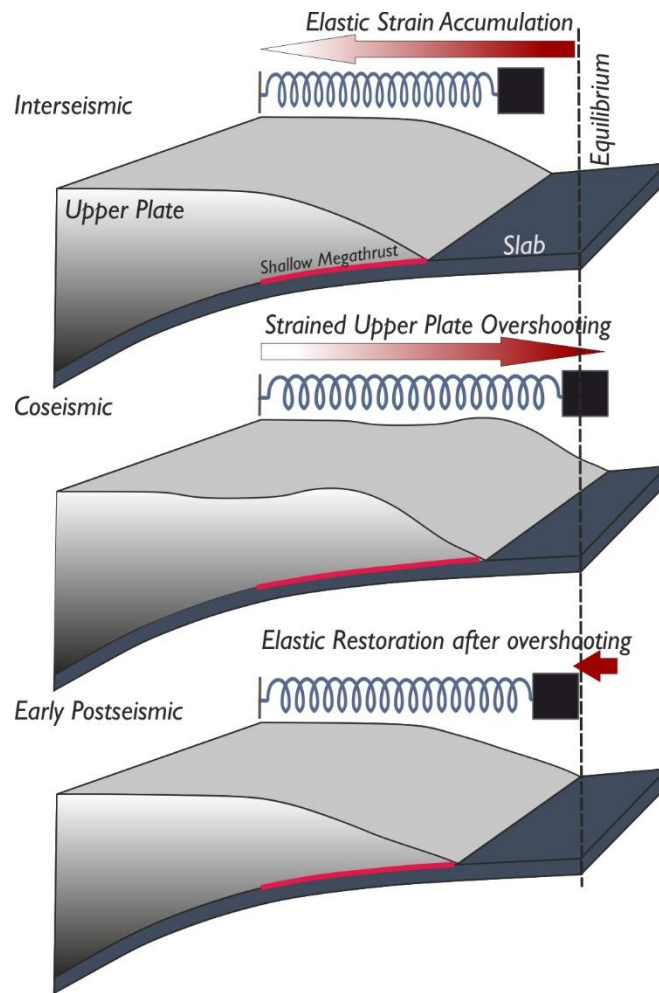
Figure S8. Schematic diagram of upper plate elastic behavior during coseismic overshooting and postseismic restoration. The interseismically strained upper plate is overshot trenchward (seaward) due to an extreme coseismic stress-drop on the interface. Subsequently, an elastic restoring force drags the upper plate back to its equilibrium state.
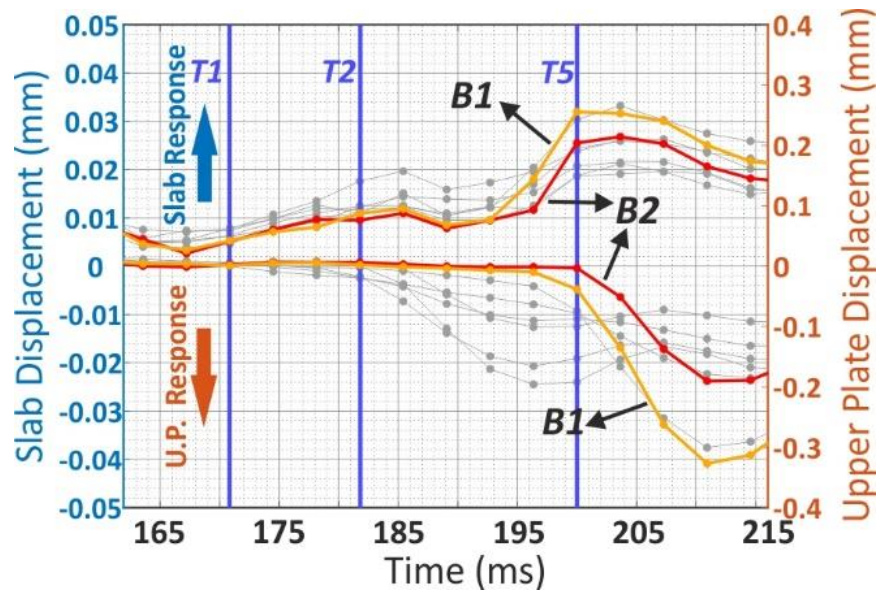
Figure S9. Timing of coseismic and postseismic elastic responses of upper plate and slab for a representative sequential event in the heterogeneous configuration. T1, T2, and T5 indicate the timing of the events in the matrix, shallow MSP, and deeper MSP, receptively. Locations of B1 and B2 can be found in Figure 4.
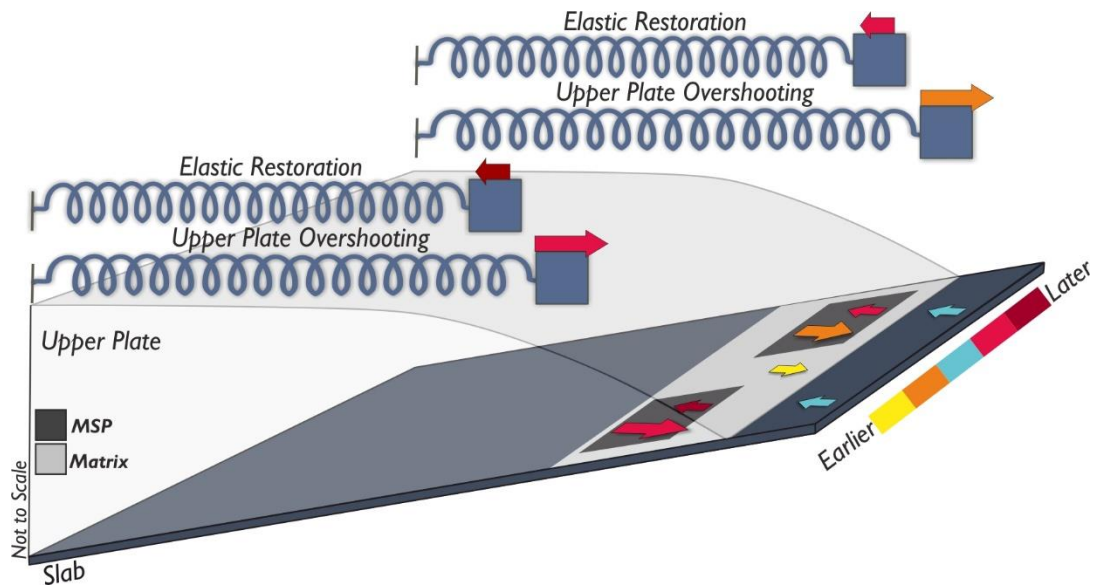
Figure S10. Schematic diagram of the sequential elastic-frictional responses of the upper plate and seismogenic zone (i.e., MSP and matrix) during coseismic and early-postseismic stages.

Text S2.

Coseismic and early postseismic upper-plate rotation

Based on the antisymmetric part of the two-dimensional velocity gradient tensor, we calculate the vertical axis rotation of the upper-plate (Figure S11, the methodology can be found in Allmendinger, Reilinger, & Loveless, 2007). The uniform and dense distribution of the observation point top of the model surface allows us to use the nearest neighbor points to calculate each point's rotation around a vertical axis. In the case of coseismic trenchward displacement of the upper plate, a divergent motion in the surface velocities above the rupture zone leads to a (sub-) symmetric vertical rotation while it may rotate the adjacent areas as well. However, there is no significant rotation above the nearby (deeper) asperity. On the other hand, in the stage that two MSPs are on opposite modes (loading vs. unloading), the surface velocities above the loading MSP show convergence mode as it may enhance the shortening rate in the early postseismic stage.
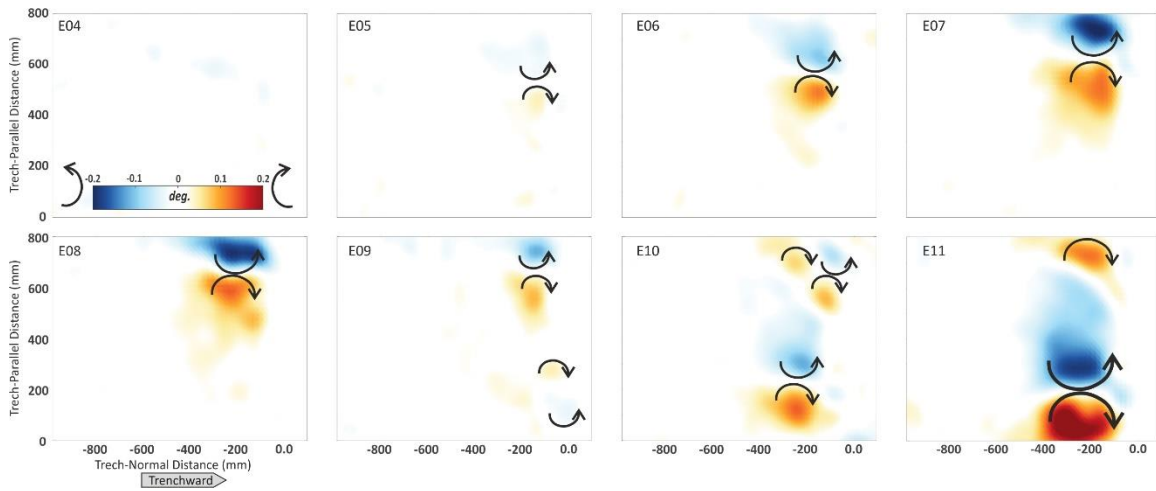

Figure S11. : Clockwise and anticlockwise upper plate rotation during coseismic and early postseismic stages derived from selected surface displacements increments. Their associated surface displacements (E04-E11) are visualized in Figure S3.

References:

Allmendinger, R. W., Reilinger, R., & Loveless, J. (2007). Strain and rotation rate from GPS in Tibet, Anatolia, and the Altiplano. *Tectonics*, *26*(3). https://doi.org/10.1029/2006TC002030

Asano, Y., Saito, T., Ito, Y., Shiomi, K., Hirose, H., Matsumoto, T., … Sekiguchi, S. (2011). Spatial distribution and focal mechanisms of aftershocks of the 2011 off the Pacific coast of Tohoku Earthquake. *Earth, Planets and Space*, *63*(7), 669–673. https://doi.org/10.5047/eps.2011.06.016

deDontney, N., Rice, J. R., & Dmowska, R. (2012). Finite element modeling of branched ruptures including off-fault plasticity. *Bulletin of the Seismological Society of America*, *102*(2), 541–562. https://doi.org/10.1785/0120110134

Hoskins, M. C., Meltzer, A., Font, Y., Agurto-Detzel, H., Vaca, S., Rolandone, F., … Rietbrock, A. (2021). Triggered crustal earthquake swarm across subduction segment boundary after the 2016 Pedernales, Ecuador megathrust earthquake. *Earth and Planetary Science Letters*, *553*, 116620. https://doi.org/10.1016/j.epsl.2020.116620

Li, S., Moreno, M., Rosenau, M., Melnick, D., & Oncken, O. (2014). Splay fault triggering by great subduction earthquakes inferred from finite element models. *Geophysical Research Letters*, *41*(2), 385–391. https://doi.org/10.1002/2013GL058598

Toda, S., Stein, R. S., & Lin, J. (2011). Widespread seismicity excitation throughout central Japan following the 2011 M=9.0 Tohoku earthquake and its interpretation by Coulomb stress transfer. *Geophysical Research Letters*, *38*(7). https://doi.org/10.1029/2011GL047834@10.1002/(ISSN)1944-8007.MEGAQUAKE1

Xu, S., Fukuyama, E., Ben-Zion, Y., & Ampuero, J. P. (2015). Dynamic rupture activation of backthrust fault branching. *Tectonophysics*, *644*, 161–183. https://doi.org/10.1016/j.tecto.2015.01.011